Universität Karlsruhe (TH)
Forschungsuniversität • gegründet 1825

Institut für Mechanik

On models of contact surfaces including anisotropy for friction and adhesion and their experimental validations

Alexander Konyukhov, Karl Schweizerhof
Universität Karlsruhe, Institut für Mechanik

Institut für Mechanik
Kaiserstr. 12, Geb. 20.30
76128 Karlsruhe
Tel.: +49 (0) 721/ 608-2071
Fax: +49 (0) 721/ 608-7990
E-Mail: ifm@uni-karlsruhe.de
www.ifm.uni-karlsruhe.de

On models of contact surfaces including anisotropy for friction and adhesion and their experimental validations

Alexander Konyukhov, Karl Schweizerhof

2006

Keywords.
Anisotropy, Adhesion, Friction, Contact, Experimental Verification.

Abstract.
A numerical model for anisotropic contact interfaces including adhesion and friction is discussed and illustrated by numerical examples. Particular attention is paid to the validation of the proposed model via experiments, where the influence of the anisotropic interface on a path of a sliding block is checked. It is shown that with the classical orthotropic Coulomb type friction model some particular kinematic effects cannot be included, while the proposed orthotropic adhesion – orthotropic friction interface model allows to qualitatively describe the observed phenomena.

1 INTRODUCTION

Smoothness and isotropy of contacting body surfaces can vary considerably for different contact problems. Classifying the surfaces roughness two types can be distinguished: a) surfaces with randomly distributed asperities, and b) asperities with algorithmic structure, e.g. the considered surface shows different macro properties in different directions.

Mechanical characteristics for the associated contact problems of the first type a) are obtained via statistically distributed asperities. Statistical analysis of a real rough surface and experimental aspects of its measurements have been developed in a series of publications: some first publications as Longuet-Higgins [1], Greenwood and Williamson [2] etc. and more recently by Greenwood [3]. A comparative analysis of these surface models is presented in McCool [4]. Such experimentally proved models later have been incorporated into finite element models, see e.g. Wriggers and Zavarise [5], Buczkowski and Kleiber [6]. More advanced numerical analyses including homogenization methods and multi-scaled modeling are presented in Bandeira et. al. [7], [8].

Constitutive modeling is applied for problems of the second type b). Such models are based on the generalization of Coulomb's friction law into the anisotropic domain. One of the first models has been proposed by Michalowski

and Mroz [9] considered the sliding of a rigid block on an inclined surface. A model of orthotropic friction has been analyzed and consistently developed in Zmitrowicz [10], see also Curnier [11]. Various cases of anisotropy were presented in He and Curnier [12] based on the theory of tensor function representations and in Zmitrowicz [13] based on the consideration of a relative sliding velocity. In the latter contribution, a classification of anisotropic surfaces based on the number of eigenvalues of the friction tensor has been proposed.

When looking at practical problems concerning friction there are some situations in which the tangential elasticity of the contact surfaces should be taken into account. Such a model including anisotropy for both friction and adhesion has been developed and analyzed numerically in Konyukhov and Schweizerhof [14] as a generalization of the computational model for isotropic friction developed in [15]. In the current contribution we discuss the validation of this model with a particular experimental test. The contact surfaces are chosen to posess elastic properties, thus a corrugated rubber mat is taken. The results of the experiments show the necessity to use a computational model including anisotropy for both friction and adhesion. Thus, some originally surprising experimental phenomena, as e.g. geometrical isotropy despite obvious physical anisotropies can be explained only within the proposed model, though the latter shows rather qualitative correlations than quantitative ones.

2 EXPERIMENTAL INVESTIGATION

A series of experimental tests is performed in order to investigate the global characteristics of the system " block on a rough surface". The rough surface has visually a clear periodical structure and, therefore, the mechanical model of an observable orthotropic structure. The focus is on the kinematical behavior of the block driven by a constant force together with the measurement of force components leading to this motion. Therefore, the main measurable characteristics in these experiments are global forces and trajectories of the block, which create a main basis for further calibration of computational models for orthotropic friction. For the judgment of the results Coulomb like models are assumed a-priori to be valid for the global behavior, i.e. that the tangential driving global force F is proportional to the normal reaction N: $F = f(x, y)N$, where a function $f(x, y)$ describes the orthotropic properties of a surface.

2.1 Experimental setup

A massive block positioned on a plane is moved with constant velocity by a sliding carriage guided by rods on both sides, see Fig. 1. The block made from steel has dimensions $110 \times 110\,mm$ in plane and $20\,mm$ height. The mass is $m = 1.875kg$. The contact surface between the sliding carriage and the block is covered with a Teflon strip to minimize the friction between them due to relative sliding. In contrast to this, the contact surface of the steel block is covered by a suede-like material with dimensions $90 \times 90\,mm$ to increase the interaction between the block and the basement. A constant driving velocity is achieved by a step motor acting on a rack, which allows a straight displacement of $500\,mm$. The contact force between the rack and the sliding carriage is measured by a force sensor. The displacement of the block during sliding is captured by an optoelectronic device which is installed on a tripod above the surface. The corresponding LED (light-emitting diode) is fixed on the block.

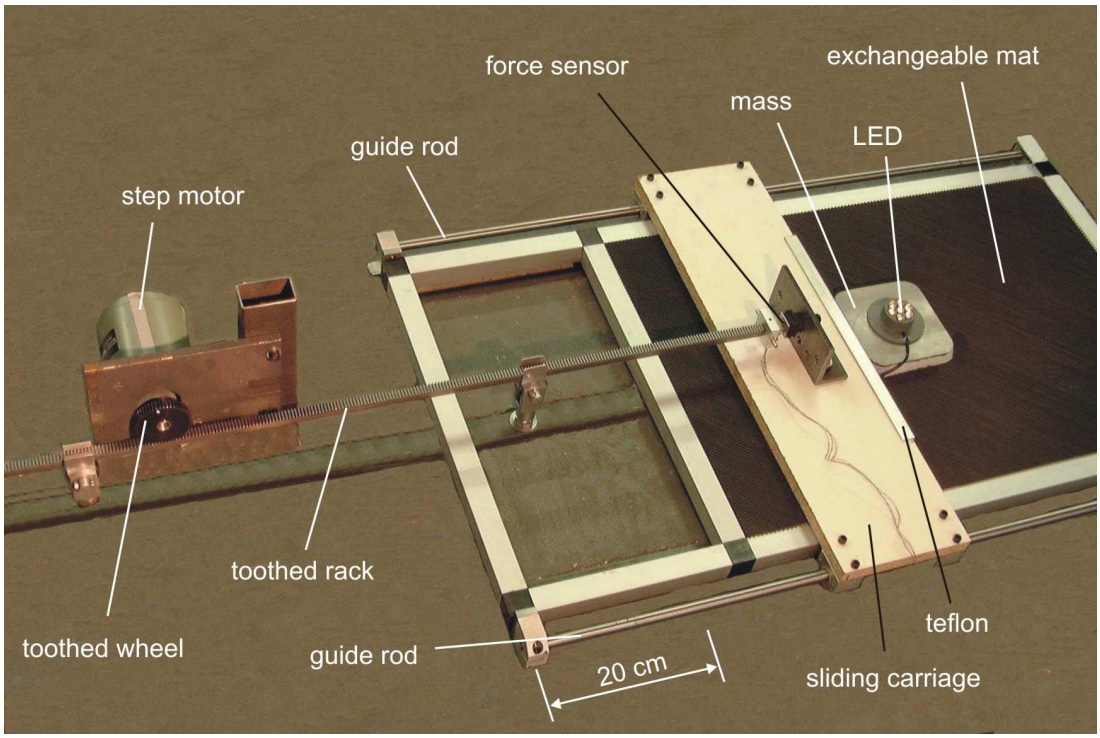

Figure 1: View on experimental setup.

For the first set of experiments an aged rubber mat (about 10 years old) is taken. The frictional orthotropy is given by the corrugation of the contact rubber surface with parallel ripples possessing in the cross section a periodical structure, see CAD model in Fig. 2. The sequence of ripples is small in comparison to the dimension of the contact area of the block. The orientation of the ripples with respect to the fixed driving direction can be varied from 0^o up

to 90^o by repositioning the mat, see Fig. 3.

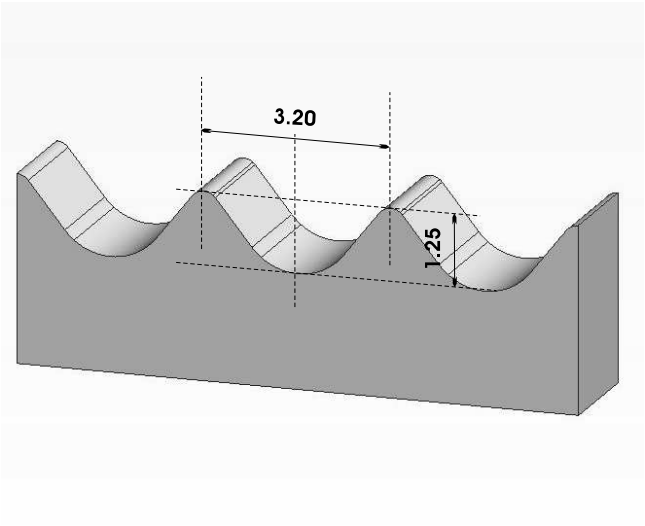

Figure 2: Geometrical structure of the corrugated rubber mat. CAD model.

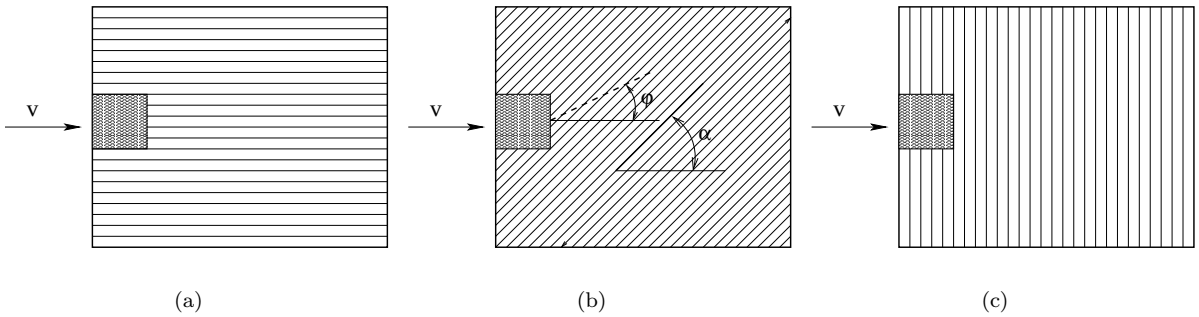

Figure 3: Orientation of the orthotropy with respect to the fixed direction of the velocity: a) $\alpha = 0^o$, b) $\alpha = 0^o < \alpha < 90^o$, c) $\alpha = 90^o$. The trajectory of the block is a straight line declined at angle φ.

2.2 Experimental results

At the beginning some experiments are performed to find out the mechanical properties of the system. All experiments were repeated twice with driving velocities of the carriage $v = 12.2\,cm/sec$ and $v = 24.4\,cm/sec$. First of all, the sliding carriage was moved without the block in order to define the internal resistant force F_{int}. Then experiments have been made with the sliding block to define the resulting driving force in the case $\alpha = 0^o$ and $\alpha = 90^o$ respectively. These measurements together with subtracting the internal force lead to the definition of friction coefficients μ_1 and μ_2 corresponding to angles $\alpha = 0^o$ and $\alpha = 90^o$. Assuming Coulomb friction the friction coefficients μ_i were computed

as

$$\begin{aligned} \mu_1 &= \frac{F_{\alpha=0^o} - F_{int}}{N} = \frac{12.50 - 5.00}{1.875 \cdot 9.806} = 0.408 \approx 0.41 \\ \mu_2 &= \frac{F_{\alpha=90^o} - F_{int}}{N} = \frac{16.50 - 5.00}{1.875 \cdot 9.806} = 0.625 \approx 0.63. \end{aligned} \tag{1}$$

The values are confirmed by repeated experiments with different velocities $v = 12.2\,cm/sec$ and $v = 24.4\,cm/sec$. The coefficient of friction proved to be independent on the applied velocity within the applied range.

The next set of experiments is made by setting the angle α varying in steps from $\alpha = 0^o$ up to $\alpha = 90^o$. The focus lies on the definition of the trajectory of the sliding block. In all cases, the trajectory is defined as a straight line inclined with angle $\varphi = \varphi(\alpha)$, see sketch in Fig. 3(b). The experiments for each angle α are repeated ten times showing negligible variance in the measured value, afterwards, the mean value φ was taken for the representation. It was also detected that the inclination angle is influenced by the sliding velocities. Combining all results leads to the diagram in Fig. 4 showing the dependency of the inclination angle φ on the orientation of the orthotropy given by the angle α of the ripples. In both cases $v = 12.2\,cm/sec$ and $v = 24.4\,cm/sec$ the maximum of the inclination angle φ is located in the range of small angles α, while the ripples are slightly inclined with respect to the angle $\alpha = 0$.

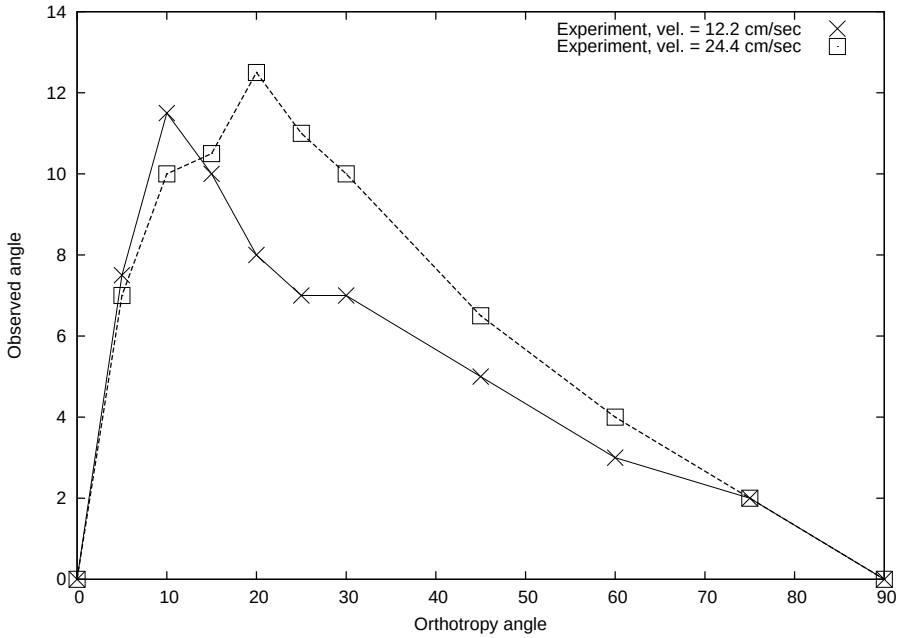

Figure 4: Observed mean value of the inclination angle φ vs. orthotropy angle α. Experimental results for different velocities of the block.

2.2.1 Controversial experimental results

As a fairly controversial result detected in the experiment a large sensitivity to the elastic properties of the rubber ripples was obtained. Thus, while repeating the last set of experiments for a new rubber mat with a notably higher elasticity in the ripples the inclination angle φ was only varying in a very small range about $0 \leq 2^o$. However, the measurement of forces still showed differences between the global coefficients of friction μ_1 and μ_2. One explanation may be that friction orthotropy is still present, but the kinematical effect of the orthotropic mat disappears, which may be confirmed better by micro- or mesoscopic models.

As we show later, the orthotropic friction model is not capable to describe this effect from the macro-model point of view, but the orthotropic adhesion – orthotropic friction interface model allows to qualitatively describe the observed phenomena.

3 ANALYSIS OF VARIOUS MODELS FOR ANISOTROPIC FRICTION AND APPLICABILITY TO THE OBSERVED PHENOMENON

In this section, the range of applicability of a classical model of orthotropic friction, based only on the orthotropic friction tensor and its generalization including orthotropy for both friction (inelastic region) and adhesion (elastic region) is discussed. The necessity to assume in addition elastic properties for the surface will be shown.

As a first simple model which can be investigated analytically a material point on a plane is considered. According to the experimental tests we assume a quasi-statical motion of the material point **A** with weight P loaded by the force **F** acting along the X^1-axis, see Fig. 5. The orthotropic properties of the surface are defined in the coordinate system ξ^1, ξ^2 inclined with an angle α to the original coordinate system. During quasi-statical loading, point **A** is moving along a line with velocity vector **v** inclined with an angle φ. The reaction force **T** with Cartesian components T_1, T_2 is acting on the point. The values of components depend on the hypothesis concerning the orthotropic friction law. Here two variants of the orthotropic law are considered: the well known orthotropic Coulomb friction law and a contact interface model including orthotropy for both friction and adhesion, see Konyukhov and Schweizerhof [14].

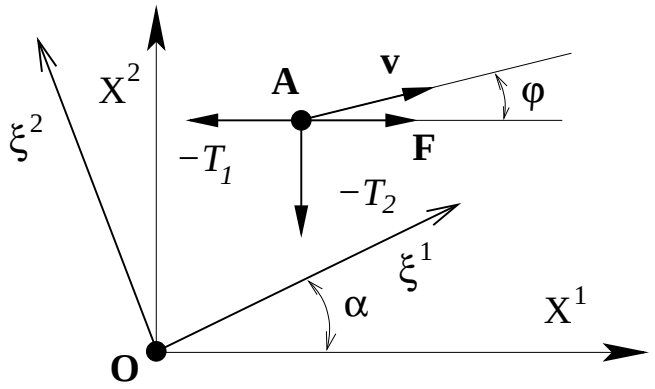

Figure 5: Motion of material point **A** on an orthotropic plane loaded by force **F**.

The equilibrium equations for the system in Fig. 5 are given as:

$$\begin{cases} X^1: & F + T_1 = 0; \\ X^2: & T_2 = 0; \\ X^3: & -P + N = 0. \end{cases}, \tag{2}$$

where N is the reaction force along the X^3 axis.

The principle of maximum dissipation is applied to obtain the sliding force $\mathbf{T}$. This principle requires that the dissipation function Ψ reaches its maximum

$$\Psi := \Delta \mathbf{r}^{sl} \cdot \mathbf{T} = \Delta x^i_{sl} T_i \longrightarrow \max, \tag{3}$$

where $\Delta \mathbf{r}^{sl}$ is an increment of the sliding vector. The dissipation function Ψ must also satisfy the sliding condition, formulated via inequalities, reflecting the assumed friction law, e.g. Coulomb's law.

3.1 Orthotropic Coulomb friction law

First, we recall the standard case known in literature, see e.g. [9], [11], [13], where orthotropy is defined only for the sliding forces. The model is formulated according to the generalization of the sliding criteria. The yield function for the Coulomb friction law is then written as

$$\Phi := \sqrt{\mathbf{T} \cdot \mathbf{F}\mathbf{T}} - |N| = \sqrt{T_i T_j f^{ij}} - |N|. \tag{4}$$

The sticking and the sliding conditions are defined by the rule:

$$\Phi < 0 \rightarrow \mathit{sticking}; \quad \Phi \geq 0 \rightarrow \mathit{sliding}. \tag{5}$$

According to equations (4-5) the material point is not moving during sticking and the motion starts when $\Phi = 0$. The components of the friction tensor f^{ij}

are defined for the orthotropy on the plane via e.g. the spectral representation plane as follows:

$$\begin{aligned}\mathbf{F} &= \mathbf{Q}_\alpha \mathbf{\Lambda}_F \mathbf{Q}_\alpha^T = \qquad (6)\\ &= \begin{bmatrix} \cos\alpha & -\sin\alpha \\ \sin\alpha & \cos\alpha \end{bmatrix} \cdot \begin{bmatrix} \dfrac{1}{\mu_1^2} & 0 \\ 0 & \dfrac{1}{\mu_2^2} \end{bmatrix} \cdot \begin{bmatrix} \cos\alpha & -\sin\alpha \\ \sin\alpha & \cos\alpha \end{bmatrix}^T \\ &= \begin{bmatrix} \dfrac{1}{\mu_1^2}\cos^2\alpha + \dfrac{1}{\mu_2^2}\sin^2\alpha & (\dfrac{1}{\mu_1^2} - \dfrac{1}{\mu_2^2})\sin\alpha\cos\alpha \\ (\dfrac{1}{\mu_1^2} - \dfrac{1}{\mu_2^2})\sin\alpha\cos\alpha & \dfrac{1}{\mu_1^2}\sin^2\alpha + \dfrac{1}{\mu_2^2}\cos^2\alpha \end{bmatrix},\end{aligned}$$

where $\mu_i > 0$ are friction coefficients along the axis ξ^i inclined at angle α.

The standard method of the convex analysis is applied to obtain the sliding forces with regard to the principle of maximum dissipation (3). Thus, the Lagrange function with the multiplier λ is specified as

$$\mathcal{L} := -\Psi + \lambda\Phi = -\Delta x_{sl}^i T_i + \lambda\left(\sqrt{T_i T_j f^{ij}} - |N|\right) \qquad (7)$$

together with the complementary Kuhn-Tucker conditions:

$$\lambda \geq 0, \quad \lambda\Phi = 0. \qquad (8)$$

The optimality conditions $\dfrac{\partial\mathcal{L}}{\partial T^i} = 0$ lead to the following sliding displacement components:

$$\Delta x_{sl}^i = \lambda \frac{T_j f^{ij}}{\sqrt{T_k T_l f^{kl}}}. \qquad (9)$$

Now, taking into account the second equilibrium equation (2) $\tan\varphi$ can be determined:

$$\left.\begin{aligned}\Delta x^1 &= \lambda \frac{T_1 f^{11}}{\sqrt{T_k T_l f^{kl}}},\\ \Delta x^2 &= \lambda \frac{T_1 f^{12}}{\sqrt{T_k T_l f^{kl}}},\end{aligned}\right\} \Longrightarrow \tan\varphi = \frac{\Delta x^2}{\Delta x^1} = \frac{f^{12}}{f^{11}}, \qquad (10)$$

and, after transformations taking into account the values determined in eqn. (6), we finally obtain:

$$\tan\varphi = \frac{(\mu_2^2 - \mu_1^2)}{\mu_2^2 + \mu_1^2\tan^2\alpha}\tan\alpha. \qquad (11)$$

3.2 Model for orthotropic contact interfaces including both adhesion and friction

An alternative model including orthotropy for both adhesion and friction can be proposed including the elastic-plastic analogy and the return-mapping scheme. This model is investigated theoretically and developed into the computational model by Konyukhov and Schweizerhof [14]. Then the problem is formulated in **continuous form** as follows

a) The relative velocity vector of the contact point is decomposed additively into an elastic part $\mathbf{v}^{el}$ and a sliding part $\mathbf{v}^{sl}$

$$\mathbf{v}^{r} = \mathbf{v}^{el} + \mathbf{v}^{sl}. \tag{12}$$

b) The elastic part $\mathbf{v}^{el}$ is responsible for reversible deformations (adhesion) and satisfies the evolution equations

$$\frac{d\mathbf{T}}{dt} = \mathbf{B}\mathbf{v}^{el}. \tag{13}$$

We have to remark that an adhesion tensor $\mathbf{B}$ describing orthotropic properties for the elastic region is introduced.

c) The tangential force $\mathbf{T}$ must satisfy the following inequalities defined via the yield function, which in tensor form can be written as:

$$\Phi := \sqrt{f^{ij}T_iT_j} - |N| = \sqrt{\mathbf{T}\cdot\mathbf{F}\mathbf{T}} - |N| : \tag{14}$$

• if $\Phi < 0$ then the contact point is inside the elastic domain and $\mathbf{T} = \mathbf{T}^{el}$ is an elastic force,
• if $\Phi = 0$ then the contact point is sliding and $\mathbf{T} = \mathbf{T}^{sl}$ is a sliding force.

d) The power of the sliding forces, described by the energy dissipation function D achieves its maximum:

$$D := \dot{x}^{i}_{sl}T^{sl}_{i} = \mathbf{v}^{sl}\cdot\mathbf{T}^{sl}, \quad D \longrightarrow \max. \tag{15}$$

The principle of maximum dissipation requires that the plastic dissipation function D subjected to the inequality conditions (14) achieves a maximum. For **the computational treatment**, the model is reformulated in **incremental form** and then the return-mapping scheme is applied. The incremental analog is given as

i) The full incremental displacement vector $\Delta x^i = \Delta x^i_{(n+1)} - \Delta x^i_{(n)}$ is decomposed additively into an elastic increment Δx^i_{el} and into a sliding increment Δx^i_{sl}:

$$\Delta x^i = \Delta x^i_{el} + \Delta x^i_{sl}. \tag{16}$$

ii) The elastic increment Δx^i_{el} is computed via the incremental evolution equations, for which the tensor $\mathbf{B}$ is assumed to be constant:

$$T^{tr}_{i\ (n+1)} = b_{ij}\Delta x^{i\ (n+1)}_{el} = b_{ij}(x^{i\ (n+1)}_{el} - x^{i\ (0)}). \tag{17}$$

iii) In order to decide whether the trial force $\mathbf{T}^{tr}$ is a sliding force $\mathbf{T}^{sl}$ or a sticking force $\mathbf{T}^{st}$ the yield condition is checked in each load step:

$$\Phi^{tr} := \sqrt{f^{ij}T^{tr}_{i\ (n+1)}T^{tr}_{j\ (n+1)}} - N_{(n+1)} \tag{18}$$

- If $\Phi^{tr} < 0$ then the trial force is a real sticking force $\mathbf{T} = \mathbf{T}^{tr}$.
- If $\Phi^{tr} \geq 0$ then the sliding force must be obtained via the maximum of the energy dissipation function given in incremental form.

iv) The incremental analog of the continuous formulation eqn. (15) is then:

$$D^{(n+1)}_{min} := -\Delta\mathbf{r}^{sl} \cdot \mathbf{T}^{sl}_{(n+1)} = -\Delta x^i_{sl} T^{sl}_{i\ (n+1)}, \quad D^{(n+1)}_{min} \longrightarrow \min. \tag{19}$$

We recall the results obtained in [14]. There the sliding force $\mathbf{T}^{sl}$ can be defined after the necessary transformations as

$$\mathbf{T}^{sl} = -\frac{\mathbf{BFT}^{tr}}{\sqrt{\mathbf{BFT}^{tr} \cdot \mathbf{FBFT}^{tr}}}|N|. \tag{20}$$

Now, we must follow the return-mapping scheme in order to define the inclination angle φ. The problem is considered as a displacement driven one, therefore the incremental displacement $\Delta\mathbf{r} = \{\Delta x^1, \Delta x^2\}$ is applied. Thus, at each load step the sliding force in eqn. (20) is computed as:

$$\mathbf{T}^{sl} = -\frac{\mathbf{BFB}\Delta\mathbf{r}}{\sqrt{\mathbf{BFT}^{tr} \cdot \mathbf{FBFT}^{tr}}}|N| = \mathbf{A}\Delta\mathbf{r}. \tag{21}$$

Now, if sliding is assumed, the second component of the sliding force T_2 in the formulation depicted in Fig. 5 becomes zero, see equilibrium eqn. (2). Thus, the displacement vector components $\Delta x^1, \Delta x^2$ are coupled via the equation:

$$T_2 = 0 \quad \Longrightarrow a_{21}\Delta x^1 + a_{22}\Delta x^2 = 0, \tag{22}$$

leading to the equation for the angle φ:

$$\tan\varphi = \frac{\Delta x^2}{\Delta x^1} = -\frac{a_{21}}{a_{22}}. \tag{23}$$

3.2.1 Analysis of the model by general spectral representation

In order to calibrate later a theoretical curve $\varphi(\alpha)$ from the experimental tests presented in Fig. 4, we consider a spectral decomposition of the matrix $\mathbf{A}$ given in eqn. (21) as

$$\mathbf{A} = [a_{ij}] = \begin{bmatrix} \lambda_1^2\cos^2\alpha + \lambda_2^2\sin^2\alpha & (\lambda_1^2-\lambda_2^2)\sin\alpha\cos\alpha \\ \\ (\lambda_1^2-\lambda_2^2)\sin\alpha\cos\alpha & \lambda_1^2\sin^2\alpha + \lambda_2^2\cos^2\alpha \end{bmatrix}, \tag{24}$$

leading together with the condition (23) to the observed sliding angle φ defined as

$$\tan\varphi = -\frac{a_{21}}{a_{22}} = -\frac{(\lambda_1^2-\lambda_2^2)\sin\alpha\cos\alpha}{\lambda_1^2\sin^2\alpha + \lambda_2^2\cos^2\alpha} = -\frac{(\lambda_1^2-\lambda_2^2)\tan\alpha}{\lambda_1^2\tan^2\alpha + \lambda_2^2}. \tag{25}$$

The analysis for extremal values gives us

$$\frac{d\tan\varphi}{d\tan\alpha} = 0, \Longrightarrow (\lambda_1^2-\lambda_2^2)(\lambda_2^2-\lambda_1^2\tan^2\alpha) = 0. \tag{26}$$

The first bracket leads to the isotropic case, whereas from the second one the following critical value is obtained:

$$\tan\alpha_{ext} = \frac{\lambda_2}{\lambda_1}, \tag{27}$$

leading to the extremum of the observed inclination angle φ_{ext} for the motion of the point

$$\tan\varphi_{ext} = \frac{\lambda_2^2-\lambda_1^2}{2\lambda_1\lambda_2}. \tag{28}$$

Considering the last equation (28) we can obtain a critical ratio of the eigenvalues

$$ratio_{ext} = \frac{\lambda_1}{\lambda_2} = -\tan\varphi_{ext} \pm \sqrt{\tan\varphi_{ext}^2 + 1}. \tag{29}$$

This value will be used during the validation procedure.

For further considerations we adopt the spectral decomposition also for the adhesion tensor

$$
\begin{aligned}
\mathbf{B} &= \mathbf{Q}_\alpha \mathbf{\Lambda}_B \mathbf{Q}_\alpha^T = \qquad (30)\\
&= \begin{bmatrix} \cos\alpha & -\sin\alpha \\ \sin\alpha & \cos\alpha \end{bmatrix} \cdot \begin{bmatrix} -\varepsilon_1 & 0 \\ 0 & -\varepsilon_2 \end{bmatrix} \cdot \begin{bmatrix} \cos\alpha & -\sin\alpha \\ \sin\alpha & \cos\alpha \end{bmatrix}^T = \\
&= \begin{bmatrix} \varepsilon_1 \cos^2\alpha + \varepsilon_2 \sin^2\alpha & (\varepsilon_1 - \varepsilon_2)\sin\alpha\cos\alpha \\ (\varepsilon_1 - \varepsilon_2)\sin\alpha\cos\alpha & \varepsilon_1 \sin^2\alpha + \varepsilon_2 \cos^2\alpha \end{bmatrix},
\end{aligned}
$$

where $\varepsilon_i > 0$ are stiffnesses along the axis ξ^i inclined at angle α.

3.2.2 Mechanical interpretation of the model

As is known, the mechanical interpretation of the regularized friction model assuming elastic deformations is a spring-slider system. As generalization of this according to our model, we consider a material point with two spring-slider systems, see Fig. 6. The properties of these system are the following: ε_i – stiffness of i^{th} spring, μ_i – coefficient of friction for i^{th} sliding device. Each system i is constrained to move parallel along the axis X_i respectively. The constant force $\mathbf{F}$ inclined with angle α to the coordinate axis X_1 is applied to the point. Then the trajectory of the point lies either above the force line or below the force line depending on the ratio of eigenvalues λ_1 and λ_2 as discussed later.

4 CALIBRATION OF PARAMETERS FOR DIFFERENT MODELS

As a representative parameter we take the curve $\varphi(\alpha)$ known from the experiment, see Fig. 4. In addition, we distinguish two orthotropy angles: α – orthotropy angle for the adhesion tensor $\mathbf{B}$ and β – orthotropy angle for the friction tensor $\mathbf{F}$. The following test computations are performed for calibration purposes:

1. The orthotropic friction model as discussed in Section 3.1.
2. The interface model including orthotropy for both adhesion and friction as discussed in Section 3.2 with the specific case of isotropic adhesion $\mathbf{B} = -\varepsilon\mathbf{E}$.
3. The interface model including orthotropy for both adhesion and friction with the specific case of isotropic friction $\mathbf{F} = \dfrac{1}{\mu^2}\mathbf{E}$.

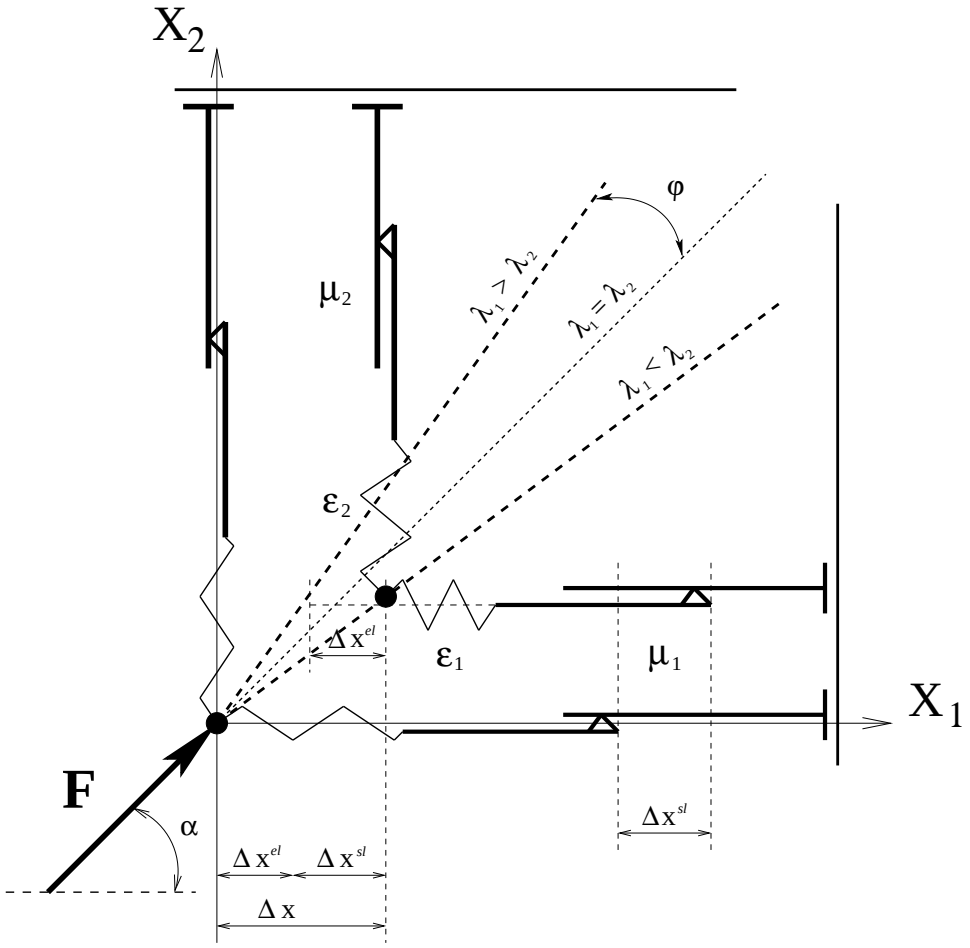

Figure 6: Mechanical interpretation of the orthotropic adhesion – orthotropic friction model. A material point on a plane with a two spring – two slider systems loaded by force **F** in plane.

4. The interface model including orthotropy for both adhesion and friction with the specific case of coinciding orthotropy angle $\alpha = \beta$.

5. The interface model including orthotropy for both adhesion and friction with the specification of the friction orthotropy angle β by 90^o degrees as $\beta = \alpha + \pi/2$.

The validation is started from the simple model including only orthotropic friction as discussed in Sect. 3.1. Our aim is to find out a case describing qualitatively the experimental results. Therefore, we perform a test computation with the following friction coefficients $\mu_1 = 0.1, \mu_1 = 0.5$. In Fig. 7 the results are depicted. In addition, at an extremal angle $\alpha = \arctan \frac{\mu_2}{\mu_1} = (78.69^o)$ the maximum value $\varphi_{\max} = \arctan \dfrac{\mu_2^2 - \mu_1^2}{2\mu_1\mu_2} = (67.38^o)$ is computed by analyzing the shape of a curve. It can be seen, that the point is moving into the direction with a smaller friction coefficient, which contradicts with the experimental curve, see Fig. 4.

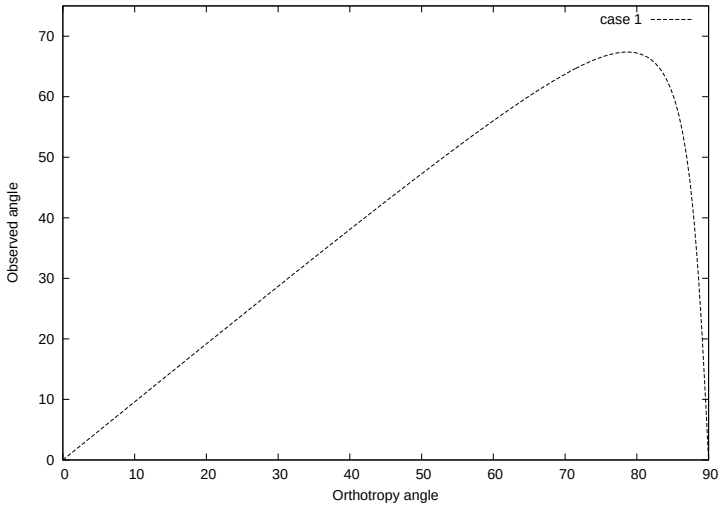

Figure 7: Computed inclination angle vs. orthotropy angle. Case 1: Purely orthotropic friction model.

Among all possible cases, the last model 5 is representing the results close to experiments. We define a new angle $\hat{\beta}$ as a main angle of surface asperities in the experiment, see Fig. 8. The orthotropy angle β for the friction tensor is shifted by 90^o degrees to $\beta = \alpha + \pi/2$ with respect to the orthotropy angle α for the adhesion tensor. The structure of the tensor $\mathbf{A}$ is given as follows:

$$\begin{aligned} \mathbf{Q}_\alpha^T \mathbf{Q}_\beta &= \\ &= \begin{bmatrix} \cos\alpha & -\sin\alpha \\ \sin\alpha & \cos\alpha \end{bmatrix}^T \cdot \begin{bmatrix} \cos\beta & -\sin\beta \\ \sin\beta & \cos\beta \end{bmatrix} = \\ &= \begin{bmatrix} \cos\alpha & -\sin\alpha \\ \sin\alpha & \cos\alpha \end{bmatrix}^T \cdot \begin{bmatrix} -\sin\alpha & -\cos\alpha \\ \cos\alpha & -\sin\alpha \end{bmatrix} = \\ &= \begin{bmatrix} 0 & -1 \\ 1 & 0 \end{bmatrix}. \end{aligned} \tag{31}$$

Then, the matrix $\mathbf{A}$ is derived as

$$\begin{aligned} \mathbf{A} = \mathbf{BFB} = \; & \mathbf{Q}_\alpha \mathbf{\Lambda}_B \underbrace{\mathbf{Q}_\alpha^T \mathbf{Q}_\beta}\, \mathbf{\Lambda}_F \underbrace{\mathbf{Q}_\beta^T \mathbf{Q}_\alpha}\, \mathbf{\Lambda}_B \mathbf{Q}_\alpha^T \\ = \; & \mathbf{Q}_\alpha \begin{bmatrix} \frac{\varepsilon_1^2}{\mu_2^2} & 0 \\ 0 & \frac{\varepsilon_2^2}{\mu_1^2} \end{bmatrix} \mathbf{Q}_\alpha^T, \end{aligned} \tag{32}$$

leading to the following eigenvalues $\lambda_1 = \varepsilon_1/\mu_2$ and $\lambda_2 = \varepsilon_2/\mu_1$ in eqn. (24). The computation with $\varepsilon_1 = 10^4$ and $\varepsilon_2 = 1 \cdot 10^3$ and $\mu_1 = 0.1, \mu_2 = 0.5$ gives the curve φ vs. $\hat{\beta}$ depicted in Fig. 9, which quantitively has a shape similar

to the experimental one. The extremal values are found as $\hat{\beta}_{ext} = 26.56^o$ and $\varphi_{\max} = 36.87^o$.

Thus, summarizing the numerical investigations and the comparison to the experiments it becomes obvious that for the surface as given in the experiment it is necessary to apply the orthotropic adhesion – orthotropic friction interface model.

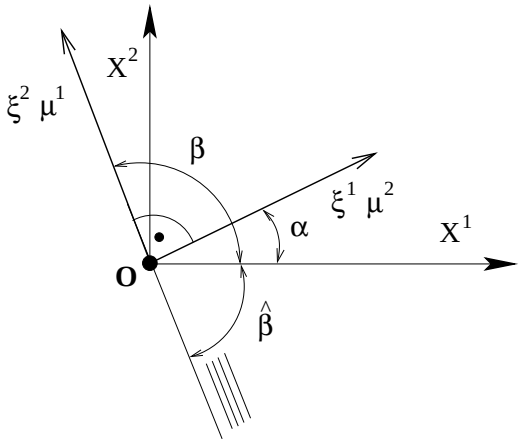

Figure 8: Definition of the experimentally observed angle $\hat{\beta}$, by an orthotropy angle α for the adhesion tensor and an orthotropy angle β for the friction tensor.

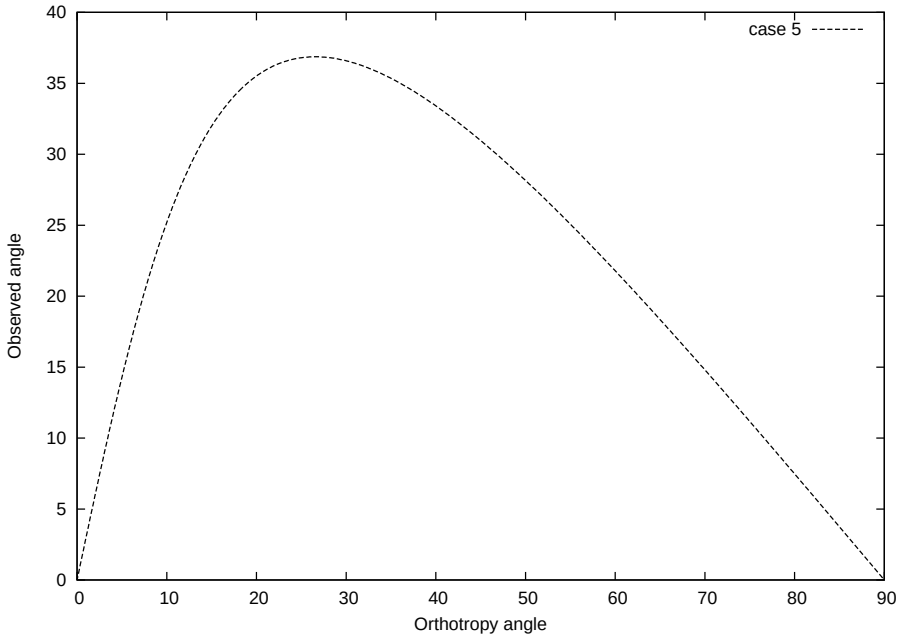

Figure 9: Orthotropic adhesion – orthotropic friction interface model. Computed inclination angle φ vs. redefined orthotropy angle $\hat{\beta}$. Case 5: orthotropic adhesion – orthotropic friction with angles $\beta = \alpha + \frac{\pi}{2}$.

4.1 Calibration of the theoretical curve by extremal values

As found from the proposed model, the inclination angle φ depends only on the ratio of eigenvalues λ_1/λ_2, see eqn. (25). This ratio contains information also about the ratio of adhesion parameters $\varepsilon_1/\varepsilon_2$:

$$ratio_{ext} = \frac{\lambda_1}{\lambda_2} = \frac{\varepsilon_1}{\varepsilon_2} \cdot \frac{\mu_1}{\mu_2}. \tag{33}$$

Since, the friction coefficients μ_1, μ_2 are defined via the measurement of forces in the experiment, the inclination angle φ depends only on the ratio of eigenvalues $\varepsilon_1/\varepsilon_2$. Thus, we will use eqn. (25) for calibration of the model. Calibration is provided according to a least square fit method. The friction coefficients have been determined previously to $\mu_1 = 0.408$, $\mu_2 = 0.625$.

The maximum value for the angle φ_{ext} defined in eqn. (29) is used for calibration purposes. Taking e.g. the maximum angle $\varphi_{\max} = 11.5^o$ measured for the velocity $12.2\,cm/sec$ the ratio of the eigenvalues given in eqn. (29) becomes

$$ratio_{ext} = \frac{\lambda_1}{\lambda_2} = -0.20345 \pm 1.02048 = 0.817, \tag{34}$$

where only the positive solution is taken. The ratio of the stiffness coefficient is then obtained as

$$\frac{\varepsilon_1}{\varepsilon_2} = \frac{\mu_2}{\mu_1} \cdot ratio_{ext} = \frac{0.625}{0.408} \cdot 0.817 = 1.251 \tag{35}$$

A more mathematically precise least square fit method leads to the statement derived from eqn. (25). The following sum must be minimized:

$$\sum_{k=1}^{N} \left\{ \tan\varphi^{(k)} + \frac{(\lambda_1^2 - \lambda_2^2)\tan\beta^{(k)}}{\lambda_1^2 \tan^2\beta^{(k)} + \lambda_2^2} \right\}^2 = \sum_{k=1}^{N} \left\{ \tan\varphi^{(k)} + \frac{(r_\lambda^2 - 1)\tan\beta^{(k)}}{r_\lambda^2 \tan^2\beta^{(k)} + 1} \right\}^2 \longrightarrow \min, \tag{36}$$

where $\varphi^{(k)}$ are measured declination angles vs. applied orthotropy angles $\alpha^{(k)}$ and $\beta^{(k)} = \pi/2 - \alpha^{(k)}$. Minimization with regard to the variable r_λ^2 leads to the following expression:

$$r_\lambda^2 = \frac{\sum_{k=1}^{N} \left\{ \tan\beta^{(k)} (1 + \tan^2\beta^{(k)})(\tan\beta^{(k)} - \tan\varphi^{(k)}) \right\}}{\sum_{k=1}^{N} \left\{ \tan\beta^{(k)} (1 + \tan^2\beta^{(k)})(\tan\beta^{(k)} + \tan\varphi^{(k)}) \right\}}. \tag{37}$$

Computation according to this rule for the case with the velocity $12.2\,cm/sec$ leads to the ratio $ratio_{ext} = 0.814$ (results close to those obtained with the maximum rule in eqn. (34).

The curves obtained for the various cases including the experimental results are shown in Fig. 10 and do not exhibit a good quantitively correlation. This

can be explained by the fact that only a simple linear elastic model for adhesion was exploited, while the experimental test was performed with rather nonlinear rubber materials. Nevertheless, it seems to be important to consider fairly complex models including orthotropy for the adhesion and for the friction in order to describe the observed phenomena correctly. This becomes obvious especially for the description of **the controversial experimental result**, see Sect. 2.2.1, where for clearly geometrically anisotropic surfaces isotropic behavior was found (in the case with a new (or young) rubber).

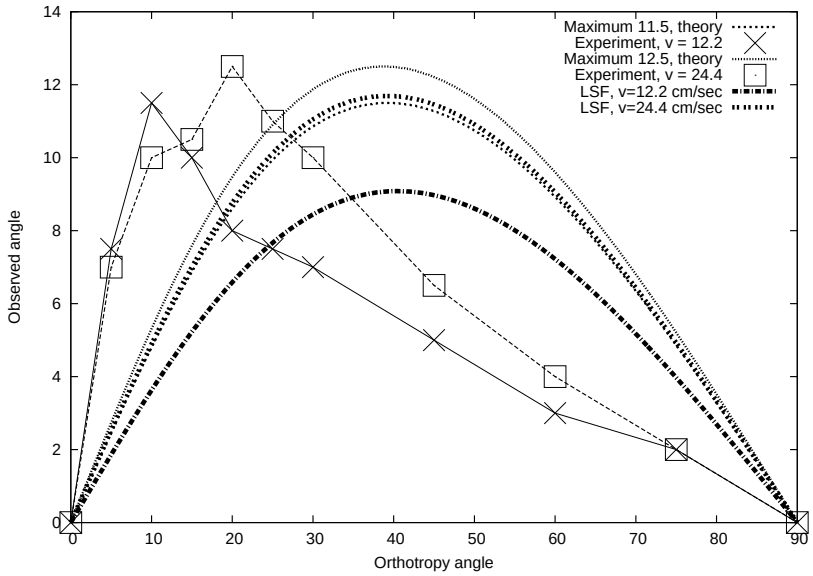

Figure 10: Observed inclination angle φ vs. redefined orthotropy angle $\hat{\beta}$. Comparison of experimental and computational results for the orthotropic adhesion – orthotropic friction model. Calibration by the least square fit method (LSF).

5 ACKNOWLEDGMENTS

We thank mechanics master W. Wendler for the careful preparation and performing of the experiments. His actions were very creative and are greatfully acknowledged. We also thank the DFG for the support given by grant SCHW 307/18-2.

6 CONCLUSIONS–OUTLOOK

A validation process for a particular contact problem with orthotropic contact surfaces possessing the elastic properties is discussed. It was shown in experiments that the classical model of orthotropic friction does not lead to a good correlation and cannot describe the particular phenomena when a sliding block shows isotropic behavior. A good qualitative result however can be achieved with the model involving both orthotropy for adhesion and for friction. The key to produce results with a closer correlation from our point of view can only be a more general law for adhesion as well as for friction. Thus, a more complex elastic law (e.g. Ogden material law for the 2D case) could be taken for the adhesion region together with a more complex friction law for the friction region (e.g. see the proposals of He and Curnier [12] and recently Zmitrowicz [16]). The calibration process, in due course, can then be supported by experimental investigations as well as by numerical tests involving homogenization processes and multi-scale techniques.

References

[1] Longuet-Higgins M. S. The statistical analysis of a random, moving surface. *Proc. of the Royal Society of London. Series A, Mathematical and Physical Sciences.* **249** (1957) 321–387.

[2] Greenwood, J. A., Williamson, J. B. P. Contact of nominally flat surfaces. *Proc. of the Royal Society of London. Series A, Mathematical and Physical Sciences.* **295** (1966) 300–319.

[3] Greenwood, J. A. A unified theory of surfaces roughness. *Proc. of the Royal Society of London. Series A, Mathematical and Physical Sciences.* **393** (1984) 133–157.

[4] McCool, John I. Comparison of models for the contact of rough surfaces. *Wear.* **107** (1986) 37–60.

[5] Wriggers, P., Zavarise, G. On the application of Augmented Lagrangian techniques for nonlinear constitutive laws in contact interface. *Communications in Applied Numerical Methods.* **9** (1993) 815–824.

[6] Buczkowski, R., Kleiber, M. Statistical model of strongly anisotropic rough surfaces for finite element contact analysis. *International Journal for Numerical Methods in Engineering.* **49** (2000) 1169–1189.

[7] Bandeira, A. A., Wriggers, P., Pimenta, P. M. Numerical derivation of contact mechanics interface laws using a finite element approach for large 3D deformation. *International Journal for Numerical Methods in Engineering.* **59** (2004) 173–195.

[8] Bandeira, A. A., Pimenta, P. M., Wriggers, P. A study of contact surface microstructure using a homogenization procedure considering elastoplastic behaviour of the asperities. *4th Contact Mechanics International Symposium. CMIS 2005, Hannover*.

[9] Michalowski, R., Mroz, Z. Associated and non-associated sliding rules in contact friction problems. *Archives of Mechanics. (Archiwum mechaniki stosowanej), Polish Academy of Sciences.* **30** (1978) 259–276.

[10] Zmitrowicz, A. A theoretical model of anisotropic dry friction. *Wear.* **73** (1981) 9–39.

[11] Curnier, A. A theory of friction. *International Journal of Solids and Structures.* **20** (1984) 637–647.

[12] He, Q.-C., Curnier, A. Anisotropic dry friction between two orthotropic surfaces undergoing large displacements. *European Journal of Mechanics A/Solids.* **12** (1993) 631–666.

[13] Zmitrowicz, A. Mathematical description of anisotropic friction. *International Journal of Solids and Structures.* **25** (1989) 837-862.

[14] Konyukhov A., Schweizerhof K. Covariant description of contact interfaces considering anisotropy for adhesion and friction. Part 1. Part 2. *Computer Methods an Applied Mechanics and Engineering.* (accepted for publication, 2006).

[15] Konyukhov A., Schweizerhof K. Covariant description for frictional contact problems. *Computational Mechanics.* **35** (2005) 190–213.

[16] Zmitrowicz, A. Models of kinematics dependent anisotropic and heterogenous friction. *International Journal of Solids and Structures*, available online 22 August 2005.